Title	Mechanochemical Stimulation of MCF7 Cells with Rod-Shaped Fe-Au Janus Particles Induces Cell Death through Paradoxical Hyperactivation of ERK
Authors(s)	Kilinc, Devrim, Lesniak, Anna, Rashdan, Suad Ahmed, Gandhi, Dhruv, Blasiak, Agata, Fannin, Paul C., Kriegsheim, Alexander von, Kolch, Walter, Lee, Gil U.
Publication date	2015-02-18
Publication information	Kilinc, Devrim, Anna Lesniak, Suad Ahmed Rashdan, Dhruv Gandhi, Agata Blasiak, Paul C. Fannin, Alexander von Kriegsheim, Walter Kolch, and Gil U. Lee. “Mechanochemical Stimulation of MCF7 Cells with Rod-Shaped Fe-Au Janus Particles Induces Cell Death through Paradoxical Hyperactivation of ERK.” Wiley, February 18, 2015. https://doi.org/10.1002/adhm.201400391.
Publisher	Wiley
Item record/more information	http://hdl.handle.net/10197/7553
Publisher's statement	This is the author's version of the following article: Devrim Kilinc, Anna Lesniak, Suad A. Rashdan, Dhruv Gandhi, Agata Blasiak, Paul C. Fannin, Alex von Kriegsheim, Walter Kolch, and Gil U. Lee (2014) "Mechanochemical Stimulation of MCF7 Cells with Rod-Shaped Fe-Au Janus Particles Induces Cell Death through Paradoxical Hyperactivation of ERK" Advanced Healthcare Materials, 4(3) : 395-404 which has been published in final form at http://dx.doi.org/10.1002/adhm.201400391.
Publisher's version (DOI)	10.1002/adhm.201400391

Mechanochemical Stimulation of MCF7 Cells with Rod-Shaped Fe-Au Janus Particles Induces Cell Death through Paradoxical Hyperactivation of ERK

Devrim Kilinc, Anna Lesniak, Suad A. Rashdan, Dhruv Gandhi, Agata Blasiak, Paul C. Fannin, Alex von Kriegsheim, Walter Kolch, and Gil U. Lee *

Dr. D. Kilinc, Dr. A. Lesniak, D. Gandhi, A. Blasiak, and Prof. G. U. Lee
UCD Nanomedicine Centre, School of Chemistry and Chemical Biology, University College Dublin, Belfield, Dublin 4, Ireland
gil.lee@ucd.ie

Dr. S. A. Rashdan
UCD Nanomedicine Centre, School of Chemistry and Chemical Biology, University College Dublin, Belfield, Dublin 4, Ireland
Department of Chemistry, University of Bahrain, P.O. Box: 32038 Sakheer, Kingdom of Bahrain

Prof. P. C. Fannin
Department of Electronic and Electrical Engineering, Trinity College Dublin, Dublin 2, Ireland

Dr. A. von Kriegsheim and Prof. W. Kolch
Systems Biology Ireland, UCD, Belfield, Dublin 4, Ireland
UCD Conway Institute, Belfield, Dublin 4, Ireland
School of Medicine and Medical Science, UCD, Belfield, Dublin 4, Ireland.

Keywords: active targeting; cancer; ErbB receptors; heregulin; magnetic hyperthermia

Multifunctional nanoparticles that actively target specific tissues are studied for cancer diagnosis and treatment. Magnetically and optically active particles are of particular interest because they enable multiple imaging modalities and physically modulated therapies, such as magnetic hyperthermia. Fe-Au nanorods are synthesized that have a long iron segment, coated with polyethylene glycol, and a short gold tip functionalized with heregulin (HRG), a known ligand of ErbB family of receptors. HRG-nanorods preferentially target MCF7 cells relative to MDA-MB-231 cells, as demonstrated in a novel microfluidics device. Targeting rates of these classical breast cancer cells correlate with their differential expression of ErbB2/3 receptors. HRG-nanorod binding stimulates the extracellular signal-regulated kinase 1/2 (ERK) phosphorylation in MCF7 cells. The increase in ERK phosphorylation is linked to 'active zones', dynamic regions in the cell periphery, which exhibit higher rates of particle binding than the rest of the cell. Periodically stretching cells using magnetic tweezers further activates ERK, which leads to cell death in cells co-treated with B-Raf inhibitors, through ERK hyperactivation. Although to a lesser extent, cell death is also achieved through magnetic hyperthermia. These results demonstrate nanoscale targeting and localized mechanochemical treatment of specific cancer cell lines based on their receptor expression using multifunctional nanoparticles.

1. Introduction

The use of nanoparticles to enhance chemotherapeutics has proven to be highly effective in preclinical and clinical studies due to their preferential uptake in tumors through enhanced permeability and retention.[1] This has led to the functionalization of nanoparticles for targeted localization to tumors to minimize the side effects of the chemotherapy.[2] Of special interest are nanoparticles that combine diagnostics with cancer therapy, acting as carriers of drugs, radionuclides, or interfering RNA.[3] For example, gold nanoparticles have proven to be excellent contrast agents for X-ray based computer tomography and near infrared (NIR) imaging when excited at their plasmon resonance frequencies. NIR radiation has also been focused to produce local heating of the gold nanoparticles,[4] causing ablation of the surrounding tissue, termed photothermal ablation therapy.[5] These particles have been used to deliver cancer drugs, such as doxorubicine,[6] or siRNA[7] in conjunction with positron emission tomography imaging and photothermal ablation therapy. Magnetic nanoparticles, on the other hand, act as contrast agents in deep tissue magnetic resonance imaging (MRI). These particles have been combined with chemotherapeutic agents,[8] and can also generate heat when exposed to alternating magnetic fields, a method known as magnetic hyperthermia therapy.[9] For example, when injected directly into the tumor site at high densities, SPIONs can generate sufficient heat to effectively treat recurrent neuroblastoma.[10] While these therapeutic methods possess inherent physical and physiological limitations, their translation to clinic is being facilitated by novel surface engineering approaches.[11]

Pierre deGennes first to describe the ‘Janus grain’, a microparticle composed of two domains, that had the capacity to self-assemble, producing materials with a number of important applications.[12] Core-shell[5, 13] and dumbbell-shaped[14] nanostructures have been produced to obtain nanoparticles that contain both Au and Fe_3O_4 functional domains. More recently, multiwalled carbon nanotubes decorated or filled with magnetic materials were produced.[15, 16] These composite nanomaterials have shown promising results for medical applications, as MRI contrast[16] or magnetic hyperthermia[15] agents. We have described the templated synthesis of Fe-Au and FePt-Au nanorods that have a high saturation magnetization (M_s), low remanence, uniform size, and strong plasmonic activity.[17, 18] The surface of the iron sections of the rods oxidize but the polycrystalline Fe cores makes these rods magnetically soft. The gold sections are typically composed of a single crystal. With tunable parameters such as size, aspect ratio, and element ratio, these nanorods provide a precise means to control the physical and chemical properties of Janus particles. The M_s of the iron section has been determined to be more than 5× higher than of superparamagnetic iron oxide nanoparticles (SPIONs),[18] which are used as MRI contrast agents.[19] Pure Fe nanoparticles have been shown to require more than 20× lower concentration to generate the same amount of heat as SPIONs of similar size[20] and hence are valuable magnetic hyperthermia therapy agents.[21] Thus, it appears pure Fe particles have the potential to replace SPIONs in targeted molecular imaging and hyperthermia, where high particle concentrations are needed to achieve the desired image contrast or heat generation, respectively.[21, 22]

Efficient *in vivo* targeting of nanoparticles has been complicated by the nature of blood and their inherently high surface energies, which leads to nonspecific protein adsorption and particle adhesion. Nanoparticle surfaces have been coated with polymers such as dextran or polyethyleneglycol (PEG), to significantly increase stability, biocompatibility and prolong blood half-life.[11, 19] Polymer coatings also increase the hydrodynamic size of the particles and spare them from being taken up by the reticulo-endothelial system.[11] To target cancer cells, nanoparticles have been further functionalized with ligands that target receptors that are over-expressed in certain types of solid tumors, *e.g.*, folate receptors *via* folic acid,[23] integrin $\alpha_v\beta_3$ *via* RGD peptide,[24] and mutant epidermal growth factor (EGF) receptor EGFRvIII *via* a specific antibody.[25] The ErbB family of receptor tyrosin kinases is also over-expressed in many cancer cells and is essential for tumor growth.[26] Individual cells have been successfully targeted with SPIONs functionalized with an antibody against ErB2 (Her2/neu).[5, 27] Heregulin (HRG) is a specific ligand of ErbB3 and ErbB4 receptors, while ErbB2 is an orphan receptor with no known ligand. However, ErbB2 is over-expressed in certain breast cancer, and can signal through heterodimerization with ErbB3.[28]

In this study we synthesized two multifunctional Fe-Au nanorods to assess their value as diagnostic and therapeutic agents. The iron section of the rods was coated with an inert layer of PEG while the gold section was functionalized with HRG. The dynamic interaction of individual nanorods with two different human breast adenocarcinoma cell lines, MCF7 and MDA-MB-231, which differentially express the ErbB family of receptors, was determined in a microfluidic chip coupled to an optical microscope with an integrated electromagnetic tweezers. This allowed us to characterize and tune the mode of interaction of the nanorods with the model cell lines and determine response of the cells to mechanical stimulation. In addition, we demonstrated two different therapeutic approaches, magnetic hyperthermia and force-induced signaling pathway hyperactivation, using specifically-targeted nanorods.

2. Results and Discussion

2.1. Synthesis and Functionalization of Fe-Au Nanorods

Fe-Au nanorods were synthesized through templated electrodeposition in nanoporous alumina membranes[18] with a diameter of 254±3 nm and Au and Fe segment lengths of 88.7±0.8 nm and 1.97±0.02 µm, respectively. **Figure 1** presents scanning and transmission electron micrographs of nanorods in which the Fe and Au segments can be clearly identified, and elemental analysis showing a sharp transition across the Fe-Au interface. As shown in Figure 1C a two-step chemistry was employed to functionalize the surface of the nanorods with a monolayer of interest.[29] The Fe segment was first coated with a silane–PEG to minimize adsorption of proteins to rods and non-specific adhesion of the rods to cells. The Au tips were then coated with a heterobifunctional thiol–PEG–carboxyl monolayer that was used to covalently immobilize streptavidin (STR) or HRG.

To verify that the functionalization was limited to the Au tips, the STR-conjugated nanorods were incubated with fluorescently-labeled biotin. Figure 1D presents the superposition of the phase contrast and fluorescence images demonstrating that STR was successfully localized to the tip of the rods. Although with lower efficiency, STR also binds to bare Au surfaces, but was not detected on Au tips coated with carboxyl-PEG (Figure S1, Table S1). The localization of STR to the Au tips was further verified by its binding to a biotinylated, fluorescently-labeled 25 bp DNA fragment, as shown in Figure 1E. When STR-conjugated nanorods were reacted with PEG-biotin surfaces, the nanorods were observed to bind irreversibly and freely follow the external magnetic field as their Au tips acted as pivot points, as shown in Figure 1F. These observations cumulatively confirm that the two-step surface chemistry employed in this study was successful in functionalizing Fe-Au nanorods with specific ligands for active targeting, while minimizing non-specific interactions. This suggests that these nanorods would be effective in targeting specific receptors as non-specific adhesion of nanoparticles is a significant factor contributing to the premature clearance of nanoparticles *in vivo*.[11] In addition, the ability to activate the Au tips allowed us to accurately control their biological activity and facilitated *in vitro* magnetic tweezers experiments in which we applied stretching forces without torque.

2.2. Specific Targeting of MCF7 Cells with HRG-Rods

Targeting of nanorods to cultured cells was determined by microscopically measuring the binding kinetic. The exceptionally high optical adsorption of the nanorods made it possible to visualize individual rods in the flow channel and on the surface of living cells with phase contrast microscopy, as shown in Figure 2A. Figure 2B and 2C present the paths of HRG-conjugated nanorods flowing over MCF7 and MDA cells, respectively, in microfluidic channels. HRG-conjugated rods that were reacted with the MCF7 cells exhibited significantly higher binding rates than those reacted with the MDA cells (Figure 2D; Movie S1-S2). There was also a significant level of interaction of STR-conjugated nanorods with MCF7 and MDA cells, which we attribute to nonspecific protein-protein interactions (Figure 2D and S2; Movies S3-S4).

ErbB2 expression on each cell type was quantified by using immunofluorescence followed by fluorescence-activated cell sorting (FACS; Figure S3). ErbB3 expression on each cell type was quantified through Western blotting. In agreement with previous studies,[30] ErbB2 and 3 expression levels were 2.3× higher in MCF7 cells than the MDA-MB-231 cells (Figure 2). The overlap between the two cell populations, in terms of ErbB2 expression, was less than one third, suggesting a low interference in the nanorod binding assays. Clearly, targeting rates of HRG-nanorods to MCF7 and MDA cells correlated with the relative ErbB2 and 3 receptor expressions in these cell types (Figure 2 and S4). Moreover, when ErbB3 was knocked-down with a pool of specific siRNAs (Figure S5), the targeting rates decreased considerably, indicating the essential role of ErbB3 in HRG-mediated targeting. These results suggest that cells over-expressing specific surface receptors can be effectively targeted with nanorods whose tips are functionalized with high densities of ligands.

A detailed microscopic analysis of particle targeting experiments revealed the non-uniform distribution of bound nanorods on cell surfaces. ‘Active zones’, dynamic extrusions in the cell periphery, attracted both HRG-conjugated rods, and to a lesser extent, STR-conjugated rods (Figure 3). HRG-conjugated rods targeted active zones six times more often than rest of the cell surface (30.7±7.9 vs. 4.9±0.8 rods per 1000 μm^2, $p < 0.005$), whereas STR-conjugated rods targeted active zones 3× more often than rest of the cell surface (18.8±4.5 vs. 6.3±0.8 rods per 1000 μm^2; $p < 0.01$). Active zones are associated with dynamic membrane ruffling and appear to exhibit a higher receptor concentration upon specific ligand binding, compared to the rest of the cell. This is consistent with the reported heterogeneities of receptor distributions, *e.g.*, ErbB receptors in MCF7 cells[31] and EGF receptors in A431 epidermoid carcinoma cells.[32] To determine if the heterogeneity in the receptor distribution is induced upon nanorod binding, we compared ErbB2 receptor staining in non-permeabilized MCF7 cells before and after targeting. Confocal micrographs show an increase in the number of receptor clusters in HRG-nanorod targeted cells compared to the controls (Figure 4; Movie S5). This suggests that localized ERK phosphorylation upon HRG-nanorod binding may be related to the localized receptor activation. On the other hand, the observation that not all receptor clusters emerged in close proximity of bound HRG-nanorods suggests that receptor clustering at remote locations may be induced by the activity of an intracellular signaling pathway.

In order to determine whether targeting of HRG-conjugated nanorods was influenced by soluble HRG in binding to MCF7 cells, the in-flow cell targeting experiment was repeated by exposing the cells to increasing concentrations of soluble HRG. Particle binding rates were not affected by the presence of free HRG up to 100 nM (Figure S6), a concentration that is two orders of magnitude higher than that needed to induce prolonged activation of mitogen-activated protein kinase/extracellular signal-regulated kinase 1/2 (MAPK/ERK) pathway in these cells.[33] The local apparent concentration of HRG on the gold tips of rods was calculated by dividing the estimated number of HRG molecules to the contact volume, which is the contact area multiplied by the estimated diameter of the molecule. The number of molecules was estimated by adjusting the previously-measured surface coverage of a similarly sized heterobifunctional PEG coated on spherical particles.[34] The local apparent density was determined to be 300 μM, which may explain the lack of competition between HRG- nanorods and soluble HRG in these experiments. Considering the (hetero) dimerization of ErbB receptors [35] and their relative HRG dissociation rates,[36] it appears that the very high local concentration of HRG at nanorod tips results in the formation of strong bonds with ErbB2/3 dimers.

Using a carrier flow to study dynamic nanoparticle-cell interactions has several advantages over traditional methods, *i.e.*, simply adding a nanoparticle suspension on top of a monolayer of cells cultured in a Petri dish. Most *in vivo* applications require the delivery of nanoparticle suspensions *via* the circulatory system, where cells and nanoparticles are in constant motion relative to each other. The use of a dynamic model system is therefore essential in understanding the active targeting mechanisms. In this work, we used a microfluidic channel to flow nanorods over cultured cells as a means to demonstrate active targeting. More precise and dynamically controlled hydrodynamic and mass transfer conditions can be achieved by implementing pressure-driven flow. In addition, microfluidic flow channels can be optimized to minimize the amount of nanorods required.

2.3. HRG-Nanorod Binding Induces Focal ERK Phosphorylation in MCF7 Cells

Rapid and prolonged activation of MAPK/ERK signaling pathway in breast cancer cells upon stimulation of ErbB2 and 3 receptors with soluble HRG has been previously shown to lead to enhanced proliferation.[33] Accordingly, soluble HRG (2 nM) induced a significant level of ERK phosphorylation within 5 min in MCF7 cells, but not MDA cells (Figure S7). In order to demonstrate the downstream intracellular signaling upon nanorod binding, ERK phosphorylation was measured in MDA and MCF7 cells targeted with STR- and HRG-conjugated rods. There was no significant change in the average pERK/ERK signal intensity ratio in the entire cell upon nanorod binding (Figure S8 and S9). However, when the analysis is restricted to active zones, ERK phosphorylation was significantly higher in MCF7 cells targeted with HRG-nanorods compared to STR-nanorods (Figure 3). Interestingly, active zones that do not have bound rods also exhibit increased ERK phosphorylation. This observation suggests a global cellular response to specific receptor activation upon nanorod binding that is pronounced in the active zones; however, further studies are required to determine the biological basis of this phenomenon.

2.4. Force Stimulation of MCF7 Cells Further Increases ERK Phosphorylation

MCF7 cells specifically targeted with HRG-nanorods were mechanically stimulated by using a custom-built magnetic tweezers coupled to a modified microfluidic device that minimized the gap between the cells in the flow channel and the electromagnet core. Cyclic stretching forces at constant magnitude were applied to cells targeted with individual rods over a fixed period of time. Cell-nanorod bonds withstood cyclic stretch at low force magnitudes but gradually failed at higher force magnitudes (Figure 5, Movie S6-S8). The rods pulled with high magnitude forces resulted in membrane tether formation, suggesting that the receptor-ligand bonds remained intact while the receptor-cytoskeleton bonds were broken. MCF7 cells had increased ERK phosphorylation when subjected to cyclic stretching at all force magnitudes tested, compared to non-stretched cells. However, ERK phosphorylation did not depend on the magnitude of the stretching force above 4.1 pN (ANOVA, $p > 0.1$). This finding may be explained by the total mechanical stimulation cells receive: Cyclic forces with low magnitudes could be transmitted to the cytoskeleton for longer periods of time, compared to the forces with higher magnitudes. Increased ERK phosphorylation is observed in the active zones as well as in the entire cell (Figure 5G). ERK phosphorylation in a particular active zone in response to cyclic stretch did not require the presence of a bound nanorod to that active zone. Interestingly, in MCF7 cells stimulated with low magnitudes of force, areas near bound nanorods which are not active zones exhibited significantly higher ERK phosphorylation, indicating that mechanotransduction was not limited to the active zones.

These results demonstrate that magnetic nanorods targeting specific membrane receptors form bonds that can withstand stretching forces. Due to the small size of the Au tips, the force will be distributed to a limited number of ErbB receptors. The mechanical load on an individual receptor may be sufficient for the activation of downstream signaling pathways, *e.g.* ERK phosphorylation. Reducing the functional area of the probe, and thereby increasing the load on individual receptors (5 pN force results in a tensile stress of 100 Pa), may be a good strategy in designing mechanotransduction probes. In this regard, magnetic rods with functionalized tips appear to be highly promising *in vivo* probes, where the force acting on a single particle may be limited due to the size of the probe and the difficulty in generating a high magnetic field gradient in the body.

2.5. Mechanical Stimulation of MCF7 Cells Treated with B-Raf Inhibitors Results in Cell Death through ERK Hyperactivation

It has been suggested that a low dose of B-Raf inhibitor would stimulate ERK activity due to induction of B-Raf/Raf-1 heterodimerization resulting in the “paradoxical” stimulation of ERK pathway.[37] Accordingly, high levels of ERK phosphorylation was observed when MCF7 cells were co-treated with 0.5–1.5 µM Vemurafenib and 0.5–1.5 µM PLX4720, both specific inhibitors of B-Raf. This effect was diminished when inhibitor concentrations were increased (Figure S10). Combined with mechanically-induced ERK phosphorylation, mild B-Raf inhibition could result in cell death by putting ERK activity into overdrive. To test this hypothesis, we applied the periodic stretch paradigm to induce local ERK phosphorylation in MCF7 cells that were pre-treated with B-Raf inhibitors. While mechanical stretch on its own did not cause any noticeable damage, mechanical stimulation combined with B-Raf inhibition resulted in cell death (Figure 6). Interestingly, higher rates of cell death was observed with low dose B-Raf inhibitors (co-treatment of 1.5 μM Vemurafenib and 1.5 μM PLX4720) compared to high dose of inhibitor treatment. These results are consistent with the paradoxical ERK stimulation in response to B-Raf pathway and with the hyperactivation scenario. Moreover, in cells treated with low dose B-Raf inhibitor, targeting of HRG-conjugated nanorods resulted in a slight, yet significant increase in the ratio of dead cells. This is consistent with the observation that HRG-mediated targeting alone induces ERK phosphorylation in MCF7 cells, albeit at lower levels compared to that induced by mechanical stimulation. (Figure 5G). This result suggests that mechanical stretching of ErbB receptors with forces as low as 4 pN can induce considerable cell damage through the activation of ERK pathway when combined with pharmaceutical interventions, leading to an overdrive of this pathway.

2.6. Alternating Magnetic Field Induces Cell Death in MCF7 Cells Targeted with Fe-Au Rods

Magnetic hyperthermia is one of the key therapeutic applications where specifically-targeted magnetic particles can be used in cancer treatment. To determine the effect of alternating magnetic field (AMF) on Fe-Au nanorods, we subjected MCF7 cells specifically targeted with HRG-conjugated rods to AMF. The frequency (f = 50–250 kHz) and amplitude (H = 1.3–6.5 A m^{-1}) of the applied field were within the range that is considered to be usable in the clinic.[38] The $f \cdot H$ product in this experiment was much lower than 5×10^{9} A m^{-1} s^{-1}, a limit recommended for the safe and tolerable magnetic fields in patients.[39]

Ferromagnetic particles show hysteresis when exposed to AMF, which results in heat generation. Heating power per unit volume can be calculated from the area of the hysteresis loop in the M–H curve by using the formula $P_{\mathrm{V}} = \mu_0 \cdot f \cdot \int M \mathrm{d}H$.[38] We observed that nanorod-targeted cells stimulated for 40 min exhibited higher levels of cell death than those stimulated for shorter periods of time (Figure 7) consistent with the amount of thermal energy they received. Rate of cell death also increased with increasing field frequency as expected from the proportional relation between field frequency and heating power. Exposure to alternating magnetic field resulted in particle agglomeration, where the size of agglomerates increased with the field frequency and the experiment duration. This suggests that the remanent magnetization of the rods was sufficient to pull them together, similar to the *in vivo* observations made by other groups.[39] This phenomenon has recently been analyzed in detail for colloidally-stable magnetic nanoparticles.[40] Particles coated with 1-5 kDa PEG formed chains during AMF application; whereas particles coated with 10-40 kDa PEG remained monodisperse following AMF application.[40] The observed agglomeration in our magnetic hyperthermia experiments may be avoided by coating the FeAu nanorods with higher molecular weight PEGs.

The hysteresis loop reported for similar Fe-Au rods[18] can be used to estimate the heating power per unit volume of the rods used in the AMF experiments. For $f = 250$ kHz and $H = 1.3$ A m^{-1}, P_V is calculated as $1.2 \cdot 10^4$ W m^{-3}. Cells used stimulated with AMF were targeted with 6.4 rods on average, corresponding to an iron mass of 5 pg per cell. Considering that the particles are localized to the cell membrane, we can approximate the effective heating volume around a single cell to a disk with a diameter of 25 µm and a thickness of 4 µm. The Fe density in this volume will be 2.5 g L^{-1}, which is an order of magnitude lower than the Fe density of the ferrofluid suspension that has been used to treat neuroblastoma.[10] This density corresponds to a specific absorption rate (SAR) value of 4.9 W g^{-1} (see Supporting Information for details). Recently, the intrinsic loss power (ILP) parameter has been introduced that normalizes the SAR value with H^2f, such that SAR values from different research groups can be compared independent of the field parameters.[41] The ILP of our rods, based on the estimated SAR, is calculated to be 11.7 nH m^2 kg^{-1}, which is higher than the best-heating synthetic particles (8.3 nH m^2 kg^{-1}).[39] However, additional studies are required to determine the absolute SAR of Fe-Au nanorods at higher f and H.

Magnetic hyperthermia has been demonstrated for small (Ø < 20 nm) nanoparticles that were internalized[20-22, 42, 43] or bound to membrane proteins.[44, 45] Here we show the induction of cell death *via* AMF heating in cells whose surface receptors were targeted, with larger Fe-Au rods. Our results suggest that considerable cell death may be induced at low particle densities which can be achieved through specific cell targeting. Recent studies demonstrated that highly localized temperature rise near magnetic nanoparticles is sufficient to affect biological processes[45] and hyperthermia-mediated cell death is achieved without a perceptible temperature rise in the medium surrounding the cells.[42] In the light of these findings, Fe-Au nanorods with strong magnetic properties may be excellent tools for *in vivo* magnetic hyperthermia applications.

3. Conclusion

Biological targeting of rod-shaped Janus particles was demonstrated for the first time. By flowing nanorods over two breast cancer cell lines, we demonstrated the highly specific targeting of cells that over-express ErbB family of receptors. The preferential binding of rods was due to high local concentration of the ligand and the avidity effect, which can outcompete very high levels of endogenous HRG. ErbB2 is over-expressed in certain breast cancer and is often linked with a poor prognosis.[28] It has been recognized that ErbB2 over-expression leads to enhanced sensitivity to specific drugs, *e.g.*, doxorubicin,[26] suggesting that Fe-Au nanorods might be useful in hyperthermia treatment used in conjunction with these drugs. Our results suggest that functionalized Fe-Au nanorods are powerful tools for targeting metastatic cancers *in vivo* for molecular imaging and therapy.

To this end, we characterized the intracellular signaling activity downstream of nanorod binding, and mechanical and thermal response of the cells to the rods. Specific targeting of ErbB family receptors resulted in focal ERK phosphorylation, which is pronounced with mechanical stimulation leading to a global cell response. Combination of mechanical stimulation with pharmaceutical inhibition of B-Raf led to cell death likely through the hyperactivation of the MAPK/ERK pathway (Figure 8). Specific targeting rather than systemic delivery of B-Raf inhibitors to cancer cells may also involve nanoparticles functionalized with alternative ligands or antibodies. Such dual targeting may further improve the specificity of the proposed mechanochemical therapy. The induction of cell death in cells targeted with a small number of nanorods and exposed to a relatively weak AMF suggested an ILP value that is higher than those reported for the best-heating particles. This is particularly important since low ILP values require high field magnitudes, which currently limits targeted hyperthermia therapies aiming to treat subclinical metastases.

Nanorods employed in this study were designed not to enter cells and this was successfully achieved. However, we had previously demonstrated that these nanorods may be easily scaled down to $d < 50$ nm,[18] which are suitable for cell internalization *in vivo*. A recent theoretical study defined the aspect ratio as a key factor in the cellular uptake of rod-shaped particles and suggested that higher aspect ratios are less favored for membrane wrapping and therefore being taken up.[46] Since the lengths of Au and Fe segments are arbitrarily controlled during synthesis, the aspect ratio of Fe-Au nanorods can be optimized for cellular uptake if needed.

There are several *in vivo* applications where the use of rod-shaped particles may be beneficial over spherical ones. For a common diameter d, a Fe-Au nanorod with an aspect ratio of $L/d = 7$ and Fe:Au segment length ratio of 17.3 (similar to the rods presented in this study) has 10× larger magnetic volume but 1.6× smaller functional surface area compared to an uniformly-functionalized spherical particle. Since the cross-sectional areas of these particles are equal, they are expected to navigate similarly in the circulatory system. Another advantage is of the cylindrical shape is that, once aligned, the nanorod will experience lower translational drag than a sphere with the same volume. This is particularly important in applications where the magnetic nanoparticles are guided to specific tissues to be used as drug carriers.[47] In summary, the strong magnetization of Fe-Au nanorods and ease of targeting makes them excellent candidates for *in vivo* molecular imaging and magnetic hyperthermia applications.

4. Experimental Section

Details of experimental procedures and materials used can be found in the Supporting Information.

Nanorod Synthesis and Surface Chemistry: The synthesis of segmented metal nanorods was based on template deposition using Al2O3 membrane filters with a pore diameter of 250 nm.[48] Ag, Au and Fe layers were electrodeposited sequentially and the segmental length of each element was controlled by monitoring the charge during deposition.[49] Following the depositions, the Ag layer was removed, the Al_2O_3 membrane was dissolved in order to release the nanorods, and the nanorods were carefully separated from solution using multiple centrifugal separations. Specific sections of the nanorods were coated with self-assembling monolayers of polyethyleneglycol (PEG) to minimize non-specific interactions.[29] The Fe segment was first coated with methoxy-PEG using silane chemistry; then, the Au segment was coated with carboxyl-PEG using thiol chemistry. Carboxylated PEG on the Au tips was subsequently functionalized with either STR or recombinant HRG by coupling their primary amines to the carboxyl groups. To confirm the localization of STR on the nanorod tips, two separate experiments were conducted. In the first experiment the rods were incubated with either fluorescein-conjugated biotin or with a biotinylated fluorescently-tagged DNA fragment. In the second experiment STR-conjugated nanorods were reacted with polystyrene surfaces that were coated with PEG-biotin.

Cell Targeting Experiments: In vitro cell targeting experiments were conducted on cells cultured in a novel microfluidic device. Polydimethylsiloxane (PDMS) microfluidic devices that have 4 mm long, 750 µm wide, and 75 µm high grooves were fabricated using photolithography and replica molding processes.[50] Inlet and outlet holes were punched out of the PDMS and the devices were permanently bonded to glass coverslips using oxygen plasma. MCF7 and MDA-MB-231 cells were seeded in UV-sterilized microfluidic devices at low confluence. Set volumes of HRG or STR-conjugated nanorod suspensions were added to the channels and flowed over the cells until the volume difference in the inlet and outlet reservoirs diminished. Nanorods with a velocity lower than 15 µm s^{-1} and with a trajectory that traverses the cell area were considered for cell targeting analysis. For HRG competition experiments, MCF7 cells in microfluidic devices were incubated with medium containing soluble HRG at varying concentrations for 15 min. HRG-conjugated rods suspended in the same medium were introduced and cell targeting was quantified as described. For ErbB3 knock-down experiments, MDA and MCF7 cells were transiently transfected with a pool of four siRNA sequences targeting ErbB3 gene. The transfection was verified through Western blotting.

Quantification of Receptor Expression and ERK Phosphorylation: Relative expression levels of ErbB2 and ErbB3 receptors in both cell types were determined by fluorescence-activated cell sorting (FACS) and western blotting, respectively, using specific antibodies. In separate experiments, the MCF7 and MDA cells targeted with HRG or STR-conjugated nanorods were immunostained against ERK and phosphorylated ERK (pERK). The level of phosphorylation was expressed in background-subtracted pERK/ERK signal intensity ratio. ERK phosphorylation in these cell lines upon stimulation with free HRG was determined using western blotting. Localization of ErbB2 receptor on MCF7 cell membranes was determined through immunocytochemistry and confocal microscopy.

Magnetic Tweezers Force Application: A custom-built electromagnet was used to apply forces on HRG-conjugated particles bound to MCF7 cells. Details of the electromagnet setup can be found in the Supporting Information. Forces acting on the nanorods were calibrated by measuring their drag velocity in fluids of defined viscosity.[51] The force is a function of the distance between the tip of the electromagnet core and the nanorod, as well as the current passing through the coil. The magnitude of the applied force for given horizontal and vertical distance from the tip and for a given current was calculated through interpolation. Acting force per nanorod in each experiment was estimated by interpolating the force values measured at known distances and currents. The multilayer design of the microfluidics chips allows us to maintain an electromagnet tip–nanorod distance no more than 500 μm, which is critical for maximizing force in the cell stretching experiments. MCF7 cells cultured in these modified devices were targeted with HRG-conjugated nanorods as described. Live cell imaging was conducted at 1.5 fps while applying periodic stretch (1 s on, 1 s off) at different force magnitudes for 15 min. Stretched cells were fixed and immunostained to determine the level of ERK phosphorylation as described. In experiments combining B-Raf inhibitor with force application, cells were pre-treated with serum-free medium containing the inhibitors for 1 h and experiments were conducted in the same medium. Following stretch experiments, the medium was removed and cells were incubated for 24 h in growth medium containing the inhibitors. In separate experiments, the induction of ERK phosphorylation in MCF7 cells treated with B-Raf inhibitors was determined through Western blotting.

Magnetic Hyperthermia Experiments: Alternating magnetic field was generated in a custom-designed multi-layered 400-turn cylindrical coil using an AC power source operating at 1 V.

The coil had an inductance of 1.6 mH, was 10 cm in length and had inner and outer diameters of 14.5 and 27 mm, respectively. MCF7 cells cultured in microfluidic devices and targeted with HRG-conjugated nanorods were introduced in the coil in tandem with cells that were not targeted (Figure S11). Microfluidic devices were positioned axially along the centre of the coil, such that each was equidistant from the centre of the coil. Following exposure to alternating magnetic field, cells were incubated in growth media for 18 h where the extent of the cell death was quantified.

Supporting Information

Supporting Information is available from the Wiley Online Library or from the author.

Acknowledgements

D. K. and A. L. contributed equally to this work.

This material is based on works supported by the Science Foundation Ireland (SFI) under grants 08/RP1/B1376 and 08/IN1/B2072 (G. U. L.), and 06/CE/B1129 (A. v. K. and W. K.) and by the Nanoremedies Programme which is funded under the Programme for Research in Third-Level Institutions and co-funded under the European Regional Development Fund. Fabrication of microfluidic masters was supported by SFI National Access Programme. S. A. R. was a recipient of Erasmus Mundus Gulf Countries Postdoctoral Fellowship and D. K. was a recipient of Marie Curie Intra-European Fellowship.

We thank Jez Simpson at UCD School of Biology and Environmental Science for confocal images. We thank Clive Downing from the Advanced Microscopy Lab at TCD for high resolution TEM and elemental analysis. We thank Emma Creagh at the Trinity Biomedical Sciences Institute, TCD, and Carlos Medina at TCD Institute of Molecular Medicine for providing access to their facilities. We thank UCD Conway Institute microscopy and FACS facilities for providing the instrumentation. We thank Joe O'Brian (Tyndall National Institute, Cork) for the fabrication of the microfluidic masters. We thank Richard Byrne and Frank Hoye (UCD College of Engineering and Architecture) for their help in building the electromagnet.

[1] Y. Matsumura, H. Maeda, *Cancer Res* **1986**, *46*, 6387.

[2] M. E. Davis, Z. G. Chen, D. M. Shin, *Nat Rev Drug Discov* **2008**, *7*, 771; J. A. Barreto, W. O'Malley, M. Kubeil, B. Graham, H. Stephan, L. Spiccia, *Adv Mater* **2011**, *23*, H18.

[3] M. P. Melancon, M. Zhou, C. Li, *Acc Chem Res* **2011**, *44*, 947.

[4] Y. Su, X. Wei, F. Peng, Y. Zhong, Y. Lu, S. Su, T. Xu, S. T. Lee, Y. He, *Nano Lett* **2012**, *12*, 1845.

[5] J. Kim, S. Park, J. E. Lee, S. M. Jin, J. H. Lee, I. S. Lee, I. Yang, J. S. Kim, S. K. Kim, M. H. Cho, T. Hyeon, *Angew Chem Int Ed Engl* **2006**, *45*, 7754.

[6] J. You, G. Zhang, C. Li, *ACS Nano* **2010**, *4*, 1033.

[7] W. Lu, G. Zhang, R. Zhang, L. G. Flores, 2nd, Q. Huang, J. G. Gelovani, C. Li, *Cancer Res* **2010**, *70*, 3177.

[8] A. Ito, M. Shinkai, H. Honda, T. Kobayashi, *Cancer Gene Ther* **2001**, *8*, 649.

[9] V. H. Ho, A. Barcza, R. Chen, K. H. Muller, N. J. Darton, N. K. Slater, *Biomaterials* **2009**, *30*, 6548.

[10] K. Maier-Hauff, R. Rothe, R. Scholz, U. Gneveckow, P. Wust, B. Thiesen, A. Feussner, A. von Deimling, N. Waldoefner, R. Felix, A. Jordan, *J Neurooncol* **2007**, *81*, 53.

[11] F. M. Kievit, M. Zhang, *Adv Mater* **2011**, *23*, H217.

[12] P. G. de Gennes, *Science* **1992**, *256*, 495; A. Walther, A. H. Muller, *Chem Rev* **2013**, *113*, 5194.

[13] L. Wang, J. Bai, Y. Li, Y. Huang, *Angew Chem Int Ed Engl* **2008**, *47*, 2439.

[14] C. Xu, J. Xie, D. Ho, C. Wang, N. Kohler, E. G. Walsh, J. R. Morgan, Y. E. Chin, S. Sun, *Angew Chem Int Ed Engl* **2008**, *47*, 173.

[15] R. Marega, F. De Leo, F. Pineux, J. Sgrignani, A. Magistrato, A. D. Naik, Y. Garcia, L. Flamant, C. Michiels, D. Bonifazi, *Adv Funct Mater* **2013**, *23*, 3173.

[16] J. T.-W. Wang, L. Cabana, M. Bourgognon, H. Kafa, A. Protti, K. Venner, A. M. Shah, J. K. Sosabowski, S. J. Mather, A. Roig, X. Ke, G. Van Tendeloo, R. T. M. de Rosales, G. Tobias, K. T. Al-Jamal, *Adv Funct Mater* **2014**, *24*, 1880.

[17] Y. Zhang, B. Ashall, G. Doyle, D. Zerulla, G. U. Lee, *Langmuir* **2012**, *28*, 17101; Y. Zhang, Q. Wang, B. Ashall, D. Zerulla, G. U. Lee, *Adv Mater* **2012**, *24*, 2485.

[18] Y. Zhang, M. DaSilva, B. Ashall, G. Doyle, D. Zerulla, T. D. Sands, G. U. Lee, *Langmuir* **2011**, *27*, 15292.

[19] J. E. Rosen, L. Chan, D. B. Shieh, F. X. Gu, *Nanomed-Nanotechnol* **2012**, *8*, 275.

[20] C. G. Hadjipanayis, M. J. Bonder, S. Balakrishnan, X. Wang, H. Mao, G. C. Hadjipanayis, *Small* **2008**, *4*, 1925.

[21] B. Mehdaoui, A. Meffre, J. Carrey, S. Lachaize, L.-M. Lacroix, M. Gougeon, B. Chaudret, M. Respaud, *Adv Funct Mater* **2011**, *21*, 4573.

[22] L. M. Lacroix, N. F. Huls, D. Ho, X. Sun, K. Cheng, S. Sun, *Nano Lett* **2011**, *11*, 1641.

[23] F. Sonvico, S. Mornet, S. Vasseur, C. Dubernet, D. Jaillard, J. Degrouard, J. Hoebeke, E. Duguet, P. Colombo, P. Couvreur, *Bioconjugate Chem* **2005**, *16*, 1181.

[24] J. Xie, K. Chen, H. Y. Lee, C. Xu, A. R. Hsu, S. Peng, X. Chen, S. Sun, *J Am Chem Soc* **2008**, *130*, 7542.

[25] C. G. Hadjipanayis, R. Machaidze, M. Kaluzova, L. Wang, A. J. Schuette, H. Chen, X. Wu, H. Mao, *Cancer Res* **2010**, *70*, 6303.

[26] S. A. Eccles, *Int J Dev Biol* **2011**, *55*, 685.

[27] D. Artemov, N. Mori, B. Okollie, Z. M. Bhujwalla, *Magn Reson Med* **2003**, *49*, 403; J. H. Lee, Y. M. Huh, Y. W. Jun, J. W. Seo, J. T. Jang, H. T. Song, S. Kim, E. J. Cho, H. G. Yoon, J. S. Suh, J. Cheon, *Nat Med* **2007**, *13*, 95.

[28] A. W. Burgess, *Growth Factors* **2008**, *26*, 263.

[29] M. Platt, G. R. Willmott, G. U. Lee, *Small* **2012**, *8*, 2436.

[30] G. Bowers, D. Reardon, T. Hewitt, P. Dent, R. B. Mikkelsen, K. Valerie, G. Lammering, C. Amir, R. K. Schmidt-Ullrich, *Oncogene* **2001**, *20*, 1388.

[31] J. Wang, X. Yu, S. V. Boriskina, B. M. Reinhard, *Nano Lett* **2012**, *12*, 3231.

[32] I. Chung, R. Akita, R. Vandlen, D. Toomre, J. Schlessinger, I. Mellman, *Nature* **2010**, *464*, 783.

[33] J. V. Thottassery, Y. Sun, L. Westbrook, S. S. Rentz, M. Manuvakhova, Z. Qu, S. Samuel, R. Upshaw, A. Cunningham, F. G. Kern, *Cancer Res* **2004**, *64*, 4637.

[34] D. Kilinc, A. Blasiak, J. J. O'Mahony, D. M. Suter, G. U. Lee, *Biophys J* **2012**, *103*, 1120.

[35] Y. Yarden, M. X. Sliwkowski, *Nat Rev Mol Cell Biol* **2001**, *2*, 127.

[36] M. Hiroshima, Y. Saeki, M. Okada-Hatakeyama, Y. Sako, *Proc Natl Acad Sci U S A* **2012**, *109*, 13984.

[37] L. K. Rushworth, A. D. Hindley, E. O'Neill, W. Kolch, *Mol Cell Biol* **2006**, *26*, 2262.

[38] Q. A. Pankhurst, J. Connolly, S. K. Jones, J. Dobson, *J Phys D: Appl Phys* **2003**, *36*, R167.

[39] S. Dutz, R. Hergt, *Int J Hyperthermia* **2013**, *29*, 790.

[40] S. L. Saville, B. Qi, J. Baker, R. Stone, R. E. Camley, K. L. Livesey, L. Ye, T. M. Crawford, O. Thompson Mefford, *Journal of Colloid and Interface Science* **2014**, *424*, 141.

[41] M. Kallumadil, M. Tada, T. Nakagawa, M. Abe, P. Southern, Q. A. Pankhurst, *J Magn Magn Mater* **2009**, *321*, 1509.

[42] M. Creixell, A. C. Bohórquez, M. Torres-Lugo, C. Rinaldi, *ACS Nano* **2011**, *5*, 7124.

[43] J. Zhang, A. H. Dewilde, P. Chinn, A. Foreman, S. Barry, D. Kanne, S. J. Braunhut, *Int J Hyperthermia* **2011**, *27*, 682.

[44] S. J. DeNardo, G. L. DeNardo, A. Natarajan, L. A. Miers, A. R. Foreman, C. Gruettner, G. N. Adamson, R. Ivkov, *J Nucl Med* **2007**, *48*, 437.

[45] H. Huang, S. Delikanli, H. Zeng, D. M. Ferkey, A. Pralle, *Nat Nano* **2010**, *5*, 602.

[46] S. Dasgupta, T. Auth, G. Gompper, *Nano Lett* **2014**, *14*, 687.

[47] Z. G. Forbes, B. B. Yellen, D. S. Halverson, G. Fridman, K. A. Barbee, G. Friedman, *IEEE Trans Biomed Eng* **2008**, *55*, 643.

[48] C. R. Martin, *Science* **1994**, *266*, 1961.

[49] S. R. Nicewarner-Pena, R. G. Freeman, B. D. Reiss, L. He, D. J. Pena, I. D. Walton, R. Cromer, C. D. Keating, M. J. Natan, *Science* **2001**, *294*, 137.

[50] D. Kilinc, J. M. Peyrin, V. Soubeyre, S. Magnifico, L. Saias, J. L. Viovy, B. Brugg, *Neurotox Res* **2011**, *19*, 149.

[51] J. Happel, H. Brenner, *Low Reynolds Number Hydrodynamics*, Prentice-Hall, Englewood Cliffs, NJ **1965**.

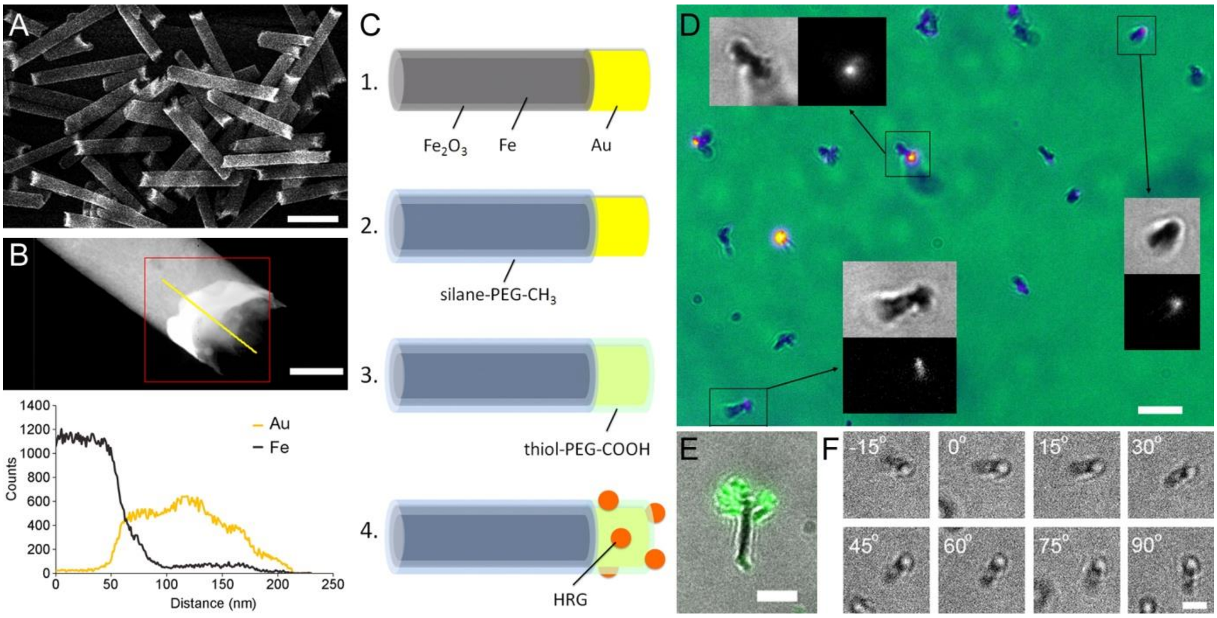

Figure 1. Synthesis of Fe-Au nanorods and characterization of their surface chemistry and physical activity. ***A.*** Scanning electron micrographs showing synthesized Fe-Au nanorods with uniform size. ***B.*** Transmission electron micrograph and energy dispersive X-ray spectroscopy analysis of the Fe-Au nanorod. The graph shows the relative element composition measured along the yellow line. ***C.*** Schematic depicting chemistry used to functionalize the rods. (1) Surface chemistry of Fe-Au nanorod, (2) Fe segment is coated with methoxy–PEG–silane monolayer, (3) Au segment is coated with carboxyl–PEG–thiol monolayer, and (4) carboxyl groups on the Au tip were coupled with the primary amines on heregulin or streptavidin. ***D.*** Streptavidin (STR)-conjugated nanorods following incubation with fluorescein-biotin. The fluorescent image was pseudo-colored and superposed with phase contrast transmission optical image. The three sets of gray scale transmission and fluorescent images are presented in 2× magnified form. ***E.*** Superposition of fluorescent and optical images of STR-conjugated nanorods that have been incubated with biotinylated fluorescein-DNA. ***F.*** Phase contrast image of a STR-conjugated nanorod rotating on a PEG-biotin surface. The rod can be seen to rotate freely around its gold tip under the influence of an external magnetic field. Scale bars = 1 µm (***A***), 100 nm (***B***), 5 µm (***D***) and 2 µm (***E***, ***F***).

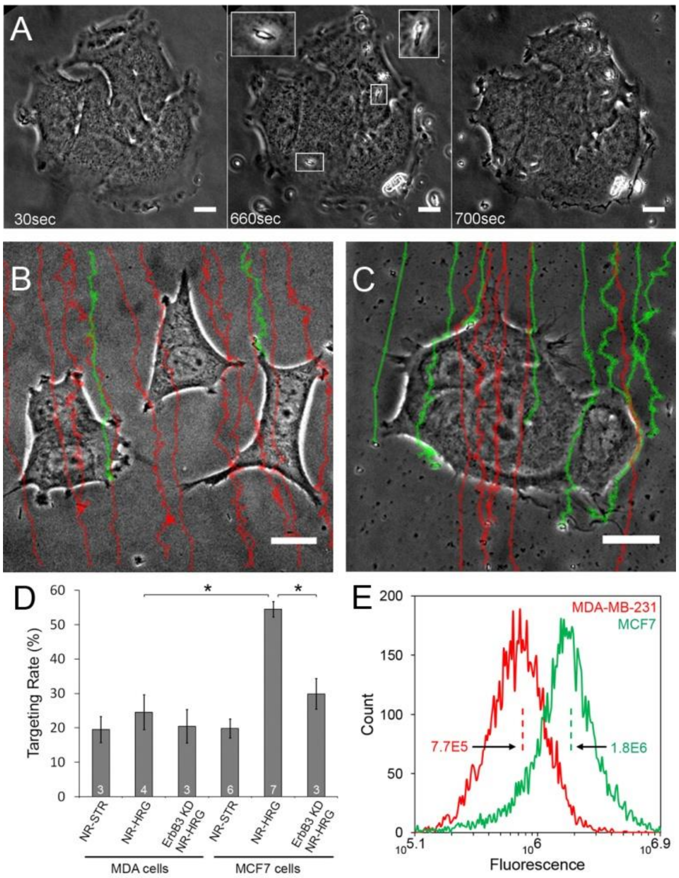

Figure 2. Nanorod targeting of breast cancer cell lines. ***A.*** MCF7 cells targeted with heregulin-conjugated Fe-Au nanorods. Time indicates seconds after particle addition. The dorsal surfaces of the cells were focused in the 660 s time frame to show individual rods attached to the cell membrane. Bars = 5 µm. Boxed areas are 2.5× magnified. ***B, C.*** Exemplary trajectories of bound (green) and passing (red) heregulin-conjugated nanorods on MDA (***B***) and MCF7 (***C***) cells. Bars = 5 µm. ***D.*** Targeting rates of HRG and STR-conjugated nanorods (NR-HRG and NR-STR, respectively) on MDA and MCF7 cells expressed as the fraction of targeted particles of total particles passing. ErbB3 KD indicates cultures that were transfected with ErbB3 siRNA. Numbers indicate the number of independent cell targeting experiments for each condition, where on average 45 particle-cell interactions analyzed per experiment. Bars indicate standard error of the mean. One-way ANOVA, followed by t-test (* $p < 0.01$). ***E.*** Relative ErbB2 expression levels for the two cell lines as measured with FACS. Note that the receptor expression levels correlate with NR-HRG targeting rates.

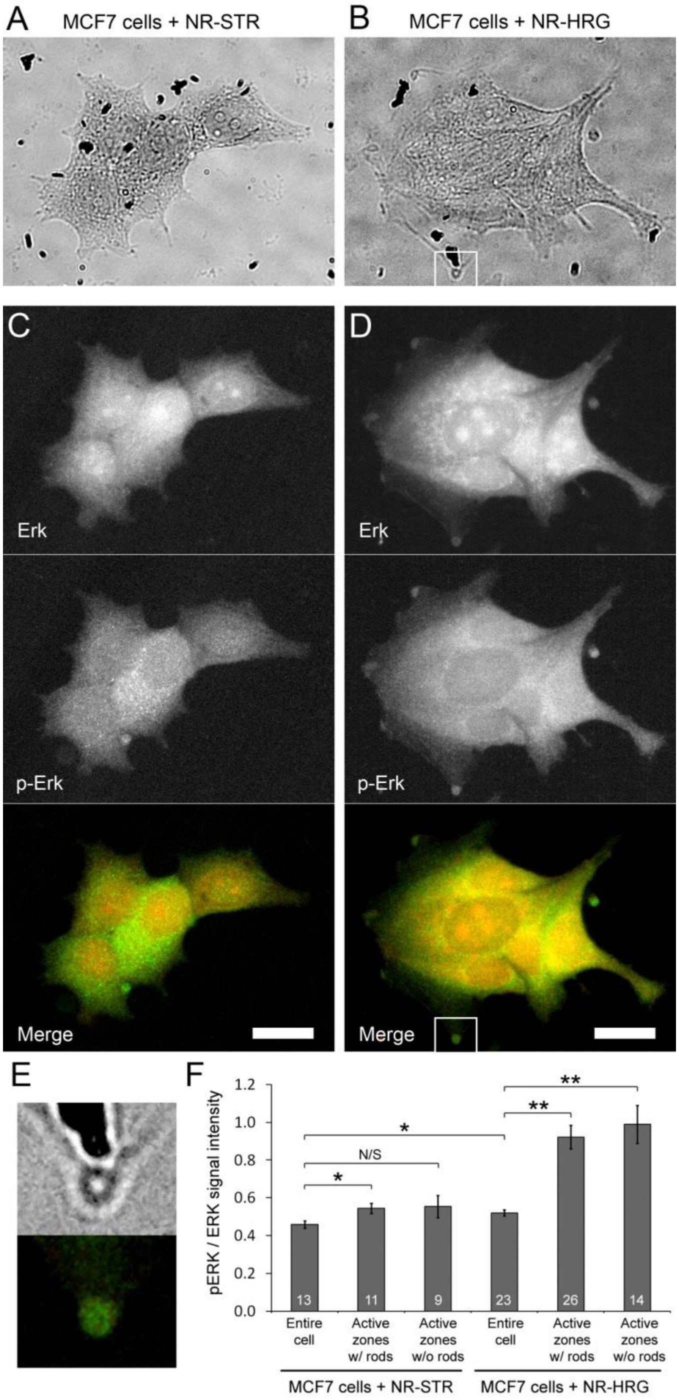

Figure 3. ERK phosphorylation in MCF7 cells in response to specific targeting. ***A, B.*** Phase contrast images of MCF7 cells targeted with HRG and STR-conjugated nanorods (NR-HRG and NR-STR, respectively). High contrast black objects are rods. ***C, D.*** ERK and pERK immunofluorescence images of the same regions. Color images are overlays of ERK (red) and pERK (green). Scale bars = 20 µm. ***E.*** Boxed areas showing an active zone, defined as having high ERK immunofluorescence, that was targeted with NR-HRG is 4× magnified. ***F.*** pERK/ERK signal intensity ratio was calculated after background subtraction. Numbers indicate the numbers of individual cells or subcellular regions analyzed for each condition. Bars indicate standard error of the mean. One-way ANOVA, followed by t-test (* $p < 0.02$; ** $p < 0.0005$). N/S: Not significant.

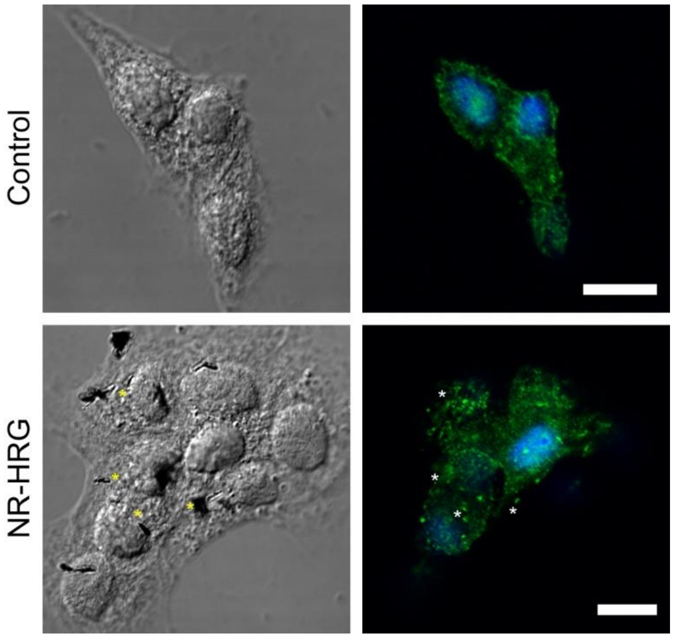

Figure 4. ErbB2 receptor clustering upon HRG-nanorod binding to MCF7 cells. Confocal micrographs showing a dorsal section of targeted (bottom panel) and non-targeted (top panel) MCF7 cells. ErbB2 receptors (green) were immunostained without permeabilizing the plasma membrane. Nuclei were stained with Hoechst 33342 (blue). Stars indicate examples of ErbB2 receptor clusters that are in close proximity of nanorods. Scale bars = 10 µm.

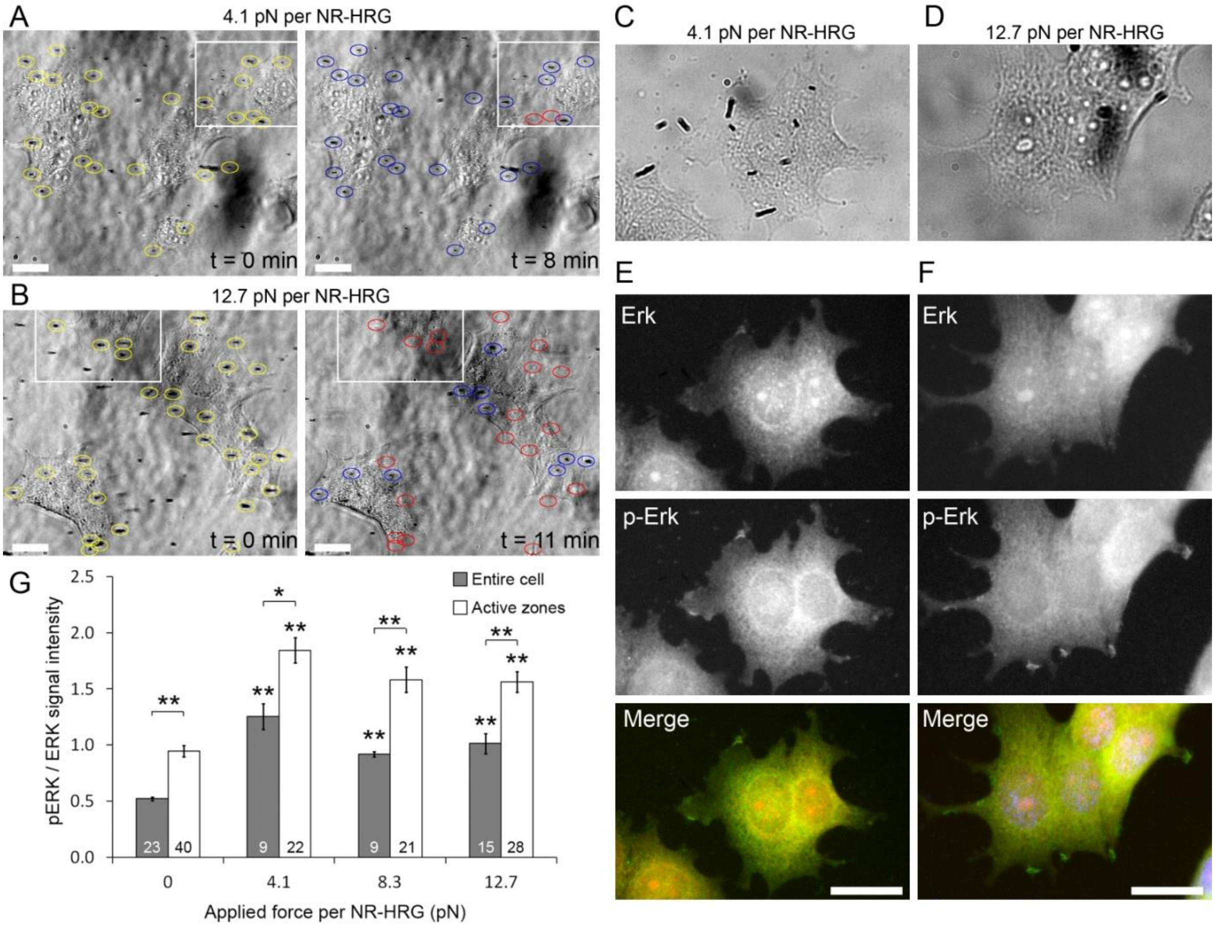

Figure 5. ERK phosphorylation in MCF7 cells targeted with HRG-conjugated nanorods (NR-HRG) and stimulated with periodic stretch. ***A, B.*** Snapshots from stretching movies, where yellow circles indicate bound nanorods immediately prior to force application (time = 0), and red and blue circles indicate escaped and remaining nanorods, respectively, at indicated time points. ***C, D.*** Images were acquired following immunocytochemistry, from the same areas that were recorded during periodic stretch experiment (boxed areas in ***A*** and ***B***). ***E, F.*** ERK and pERK immunofluorescence images of the same regions. Color images are overlays of ERK (green) and pERK (red). Scale bars = 20 µm. ***G.*** pERK/ERK signal intensity ratio after background subtraction. Numbers indicate the numbers of individual cells or subcellular regions analyzed for each condition. Bars indicate standard error of the mean. One-way ANOVA, followed by t-test (* $p < 0.005$; ** $p < 0.0005$). pERK/ERK ratio at each force level is statistically significant compared to zero force condition. pERK/ERK ratio among different force levels is not significant in the entire cell ($p > 0.06$) and in active zones ($p > 0.11$).

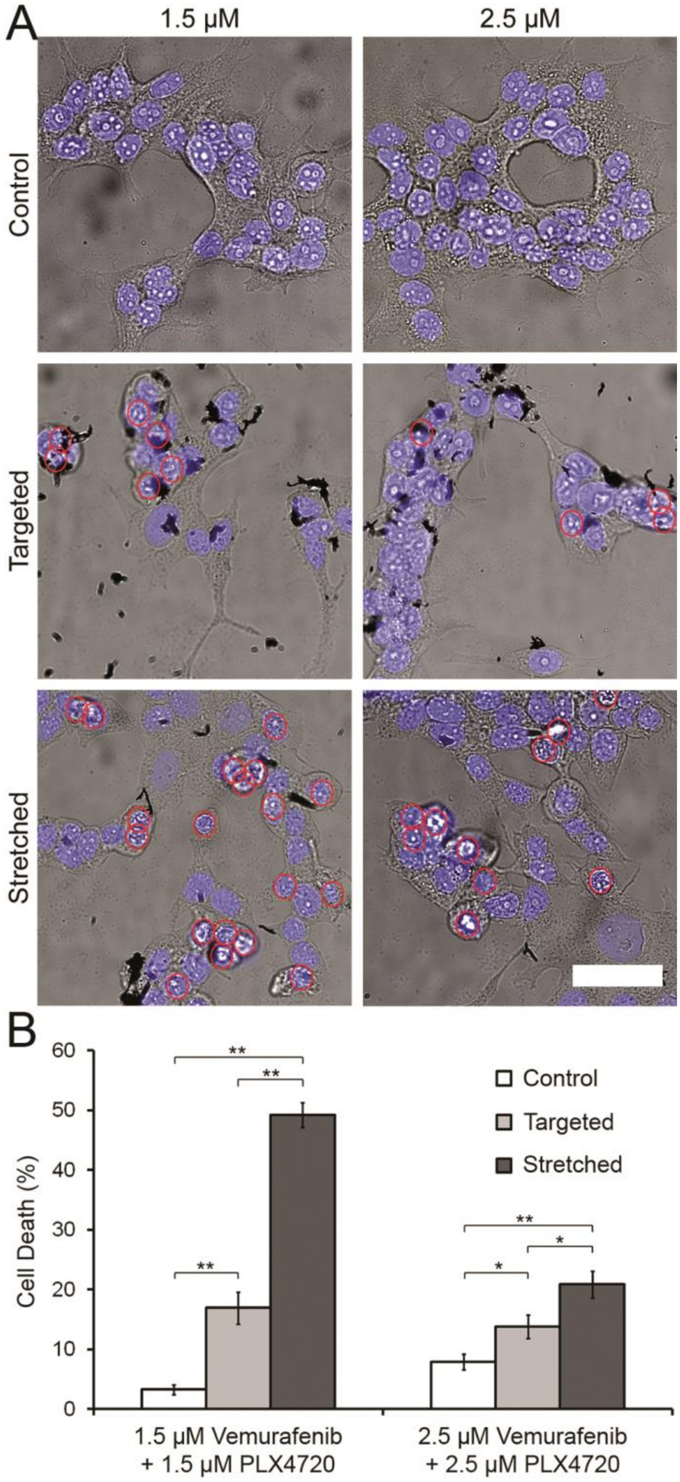

Figure 6. MCF7 cell death in response to specific targeting and mechanical stimulation combined with B-Raf inhibition. ***A.*** Overlays of phase contrast images and nuclear stains (blue) of MCF7 cells: Intact; targeted with HRG-conjugated nanorods; and periodically stretched after targeting. High contrast black objects are rods. Red circles indicate dead cells. Column headings indicate the concentration of each inhibitor in the co-treatment. Scale bar = 40 µm. ***B.*** Cell death was determined by dense nuclear staining and atypical cell shape. More than 300 cells in two independent experiments were analyzed for each condition. Bars indicate standard error of the mean. One-way ANOVA, followed by t-test (* $p < 0.05$; ** $p < 0.0005$).

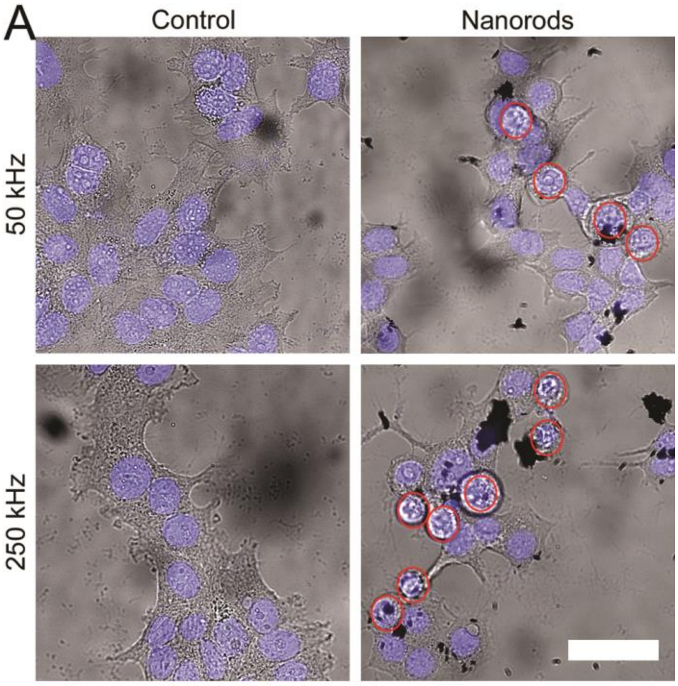

B

f (kHz)	50			250		
T (min)	10	20	40	10	20	40
Control	2.7	5.3	3.9	5.7	6.3	2.9
Nanorods	6.1	4.7	21.2	10.9	1.5	30.0

Figure 7. MCF7 cell death in response to stimulation with alternating magnetic field (AMF). ***A.*** Overlays of phase contrast images and nuclear stains (blue) of MCF7 cells targeted with HRG-conjugated nanorods and subjected to AMF at indicated frequencies for 40 min. Control cells underwent the same protocol except particle targeting. High contrast black objects are rods. Red circles indicate dead cells. Scale bar = 40 µm. ***B.*** Cell death (%) was determined by dense nuclear staining and atypical cell shape for cells exposed to the field for 10, 20, or 40 min. Field frequency and exposure are denoted as *f* and *T*, respectively. More than 100 cells were analyzed for each condition.

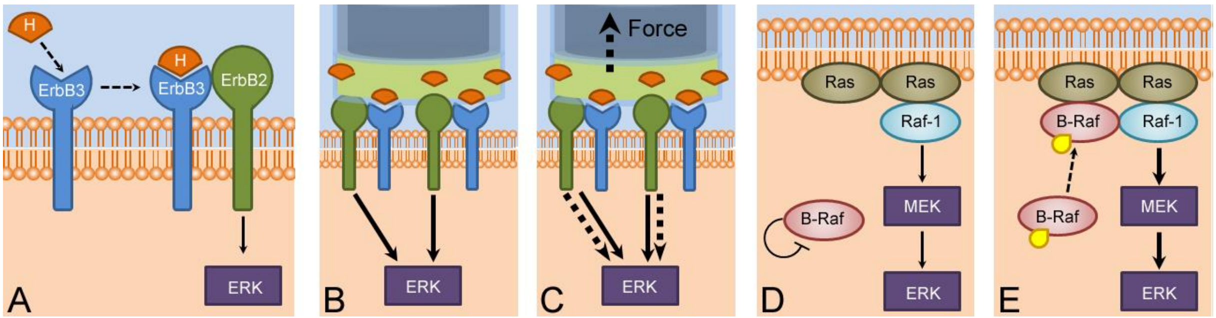

Figure 8. Putative molecular mechanisms downstream of mechanical stimulation and pharmaceutical intervention in MCF7 cells. ***A.*** HRG (H) binds to ErbB3 receptors, which in turn form heterodimers with ErbB2 receptors to activate several intracellular signaling pathways including ERK pathway. ***B.*** Specific binding of HRG-conjugated Fe-Au nanorods results in receptor clustering and increased ERK phosphorylation in 'active zones'. ***C.*** Periodic stretch with externally applied force further increases ERK phosphorylation. ***D.*** Signals downstream of receptor binding sequentially activate Ras, Raf-1 and MEK, where B-Raf is auto-inhibited. ***E.*** Low dose B-Raf inhibitor (yellow shape) blocks the auto-inhibition and B-Raf forms a complex with Raf-1 resulting in enhanced MEK and ERK activation. B-Raf inhibition in combination with mechanical stimulation of ErbB receptors appears to lead to ERK hyperactivation resulting in cell death.

Iron nanorods with heregulin-functionalized gold tips preferentially target MCF7 cells compared to MDA-MB-231 cells where targeting rates correlate relative ErbB3 receptor expression levels. Nanorod binding induces localized ERK phosphorylation, which is pronounced when cells are periodically stretched. Co-treatment with B-Raf inhibitors results in cell death through ERK hyperstimulation, demonstrating the nanoscale targeting and localized mechanochemical treatment of specific cancer cells.

Fe-Au nanorods

D. Kilinc, A. Lesniak, S. A. Rashdan, D. Gandhi, A. Blasiak, P. C. Fannin, A. von Kriegsheim, W. Kolch, and G. U. Lee*

Mechanochemical Stimulation of MCF7 Cells with Rod-Shaped Fe-Au Janus Particles Induces Cell Death through Paradoxical Hyperactivation of ERK